Cluster multipole theory for anomalous Hall effect in antiferromagnets

M.-T. Suzuki, T. Koretsune, M. Ochi, and R. Arita

Phys. Rev. B **95**, 094406 — Published 7 March 2017

DOI: 10.1103/PhysRevB.95.094406

Cluster multipole theory for anomalous Hall effect in antiferromagnets

M.-T. Suzuki,[1] T. Koretsune,[1,2] M. Ochi,[3] and R. Arita[1]

[1]*RIKEN Center for Emergent Matter Science (CEMS), Wako, Saitama 351-0198, Japan*

[2]*JST, PRESTO, 4-1-8 Honcho Kawaguchi, Saitama 332-0012, Japan.*

[3]*Department of Physics, Osaka University, Toyonaka, Osaka 560-0043, Japan*

(Dated: February 13, 2017)

We introduce a cluster extension of multipole moments to discuss the anomalous Hall effect (AHE) in both ferromagnetic (FM) and antiferromagnetic (AFM) states in a unified framework. We first derive general symmetry requirements for the AHE in the presence or absence of the spin-orbit coupling, by considering the symmetry of the Berry curvature in $\boldsymbol{k}$ space. The cluster multipole (CMP) moments are then defined to quantify the macroscopic magnetization in non-collinear AFM states, as a natural generalization of the magnetization in FM states. We identify the macroscopic CMP order which induces the AHE. The theoretical framework is applied to the non-collinear AFM states of Mn_3Ir, for which an AHE was predicted in a first-principles calculation, and Mn_3Z (Z=Sn, Ge), for which a large AHE was recently discovered experimentally. We further compare the AHE in Mn_3Z and bcc Fe in terms of the CMP. We show that the AHE in Mn_3Z is characterized with the magnetization of a cluster octupole moment in the same manner as that in bcc Fe characterized with the magnetization of the dipole moment.

I. INTRODUCTION

The modern formalism of the intrinsic anomalous Hall conductivity (AHC) provides profound insight into the anomalous Hall effect (AHE) of being closely related with the topology of one-electron energy bands[1–3]. The AHE is usually observed in ferromagnetic (FM) metals, but the AHE has been studied also for certain non-collinear antiferromagnetic (AFM) states[1,4–13]. Especially, a large AHC has been recently discovered for the AFM states in Mn_3Z (Z=Sn, Ge), whose magnetic geometry has no uniform magnetization[14–16]. The topological feature of these AFM states has also been investigated based on the first-principles calculations[12,13,17].

The AHE requires not only the broken time-reversal symmetry but also a certain type of magnetic structure[18,19]. Furthermore, the situation changes depending on the presence or absence of the spin-orbit (S-O) coupling. For instance, the AHE requires the S-O coupling in collinear FM states, characterized by uniform magnetization. The crucial role of the S-O coupling for the AHE in the FM states has been discussed since its pioneering work[20]. On the other hand, in AFM systems, two types of AHE have been investigated. One is the AHE in non-coplanar spin configurations where the AHE can be induced even without the S-O coupling. The AHE is characterized by the scalar spin chirality[21] and studied intensively in the context of the topological Hall effect[6,22]. The other is the AHE in coplanar spin systems such as Mn_3Sn[12,13,23]. In this case, it is not well understood whether there is a macroscopic quantity that characterizes the AHE such as the uniform magnetization or scalar spin chirality. Moreover, there is no clear explanation for what types of AFM structures induce the AHE.

The purpose of this paper is to provide comprehensive understanding of the AHE in relation to the magnetic structure. We propose a new order parameter, which we call the cluster multipole (CMP) moment, to measure the symmetry breaking of commensurate non-collinear magnetic order. This systematically explains what types of AFM structures induce the AHE and whether the AHE requires the S-O coupling or not in that AFM state.

The structure of this paper is as follows. In Sec. II, we derive a symmetry condition for finite AHC in generic non-collinear magnetic systems by considering the symmetry of the Berry curvature in $\boldsymbol{k}$ space. We show that the AHE is forbidden to emerge by some symmetry elements of the magnetic space group, whose operations preserve the magnetic structure. The derivation also leads to comprehensive understanding for the requirement of the S-O coupling for the AHE. In Sec. III, we introduce CMP moments as order parameters defined for a cluster of atoms, which is a natural generalization of the local magnetic moments for atoms. The CMP characterizes the non-collinear AFM structure as analogous to the atomic magnetic multipole moments characterizing the local magnetic distribution[24–29]. We show that the AHE of Mn_3Ir and Mn_3Z is associated with the cluster octupole moments which belong to the same symmetry with the magnetic dipole moments. In Sec. IV, we calculate the electronic structure, Berry curvature and AHC for the AFM states of Mn_3Z from first principles. As a reference, we also calculated those properties for the FM state of bcc-Fe, which has well been investigated in earlier works[30–32]. We show that the AHE of the FM and AFM states can be discussed in the same framework in terms of the CMP. Finally, a summary of the results is given in Sec. V.

TABLE I. Constraint on the Berry curvature in $\boldsymbol{k}$ space for some representative symmetries. The x, y, z express the Cartesian coordinates. $C_{n\mu}$ indicates the n-fold rotation operator along the μ-axis, P is the spacial inversion operator, and T is the time reversal operator. Mirror operation whose mirror plane normal to the μ-axis corresponds to $PC_{2\mu}$.

Unitary operators		Anti-unitary operators	
C_{2z}	$\Omega^x(-k_x,-k_y,k_z)=-\Omega^x(k_x,k_y,k_z)$ $\Omega^y(-k_x,-k_y,k_z)=-\Omega^y(k_x,k_y,k_z)$ $\Omega^z(-k_x,-k_y,k_z)=\Omega^z(k_x,k_y,k_z)$	TC_{2z}	$\Omega^x(k_x,k_y,-k_z)=\Omega^x(k_x,k_y,k_z)$ $\Omega^y(k_x,k_y,-k_z)=\Omega^y(k_x,k_y,k_z)$ $\Omega^z(k_x,k_y,-k_z)=-\Omega^z(k_x,k_y,k_z)$
PC_{2z}	$\Omega^x(k_x,k_y,-k_z)=-\Omega^x(k_x,k_y,k_z)$ $\Omega^y(k_x,k_y,-k_z)=-\Omega^y(k_x,k_y,k_z)$ $\Omega^z(k_x,k_y,-k_z)=\Omega^z(k_x,k_y,k_z)$	TPC_{2z}	$\Omega^x(-k_x,-k_y,k_z)=\Omega^x(k_x,k_y,k_z)$ $\Omega^y(-k_x,-k_y,k_z)=\Omega^y(k_x,k_y,k_z)$ $\Omega^z(-k_x,-k_y,k_z)=-\Omega^z(k_x,k_y,k_z)$
$C_{2[1\bar{1}0]}$	$\Omega^x(-k_y,-k_x,-k_z)=-\Omega^y(k_x,k_y,k_z)$ $\Omega^y(-k_y,-k_x,-k_z)=-\Omega^x(k_x,k_y,k_z)$ $\Omega^z(-k_y,-k_x,-k_z)=-\Omega^z(k_x,k_y,k_z)$	$TC_{2[1\bar{1}0]}$	$\Omega^x(k_y,k_x,k_z)=\Omega^y(k_x,k_y,k_z)$ $\Omega^y(k_y,k_x,k_z)=\Omega^x(k_x,k_y,k_z)$ $\Omega^z(k_y,k_x,-k_z)=\Omega^z(k_x,k_y,k_z)$
$PC_{2[1\bar{1}0]}$	$\Omega^x(k_y,k_x,k_z)=-\Omega^y(k_x,k_y,k_z)$ $\Omega^y(k_y,k_x,k_z)=-\Omega^x(k_x,k_y,k_z)$ $\Omega^z(k_y,k_x,k_z)=-\Omega^z(k_x,k_y,k_z)$	$TPC_{2[1\bar{1}0]}$	$\Omega^x(-k_y,-k_x,-k_z)=\Omega^y(k_x,k_y,k_z)$ $\Omega^y(-k_y,-k_x,-k_z)=\Omega^x(k_x,k_y,k_z)$ $\Omega^z(-k_y,-k_x,-k_z)=\Omega^z(k_x,k_y,k_z)$
$C_{3[111]}$	$\Omega^x(k_z,k_x,k_y)=\Omega^y(k_x,k_y,k_z)$ $\Omega^y(k_z,k_x,k_y)=\Omega^z(k_x,k_y,k_z)$ $\Omega^z(k_z,k_x,k_y)=\Omega^x(k_x,k_y,k_z)$	$TC_{3[111]}$	$\Omega^x(-k_z,-k_x,-k_y)=-\Omega^y(k_x,k_y,k_z)$ $\Omega^y(-k_z,-k_x,-k_y)=-\Omega^z(k_x,k_y,k_z)$ $\Omega^z(-k_z,-k_x,-k_y)=-\Omega^x(k_x,k_y,k_z)$
$PC_{3[111]}$	$\Omega^x(-k_z,-k_x,-k_y)=\Omega^y(k_x,k_y,k_z)$ $\Omega^y(-k_z,-k_x,-k_y)=\Omega^z(k_x,k_y,k_z)$ $\Omega^z(-k_z,-k_x,-k_y)=\Omega^x(k_x,k_y,k_z)$	$TPC_{3[111]}$	$\Omega^x(k_z,k_x,k_y)=-\Omega^y(k_x,k_y,k_z)$ $\Omega^y(k_z,k_x,k_y)=-\Omega^z(k_x,k_y,k_z)$ $\Omega^z(k_z,k_x,k_y)=-\Omega^x(k_x,k_y,k_z)$

II. SYMMETRY ASPECT OF ANOMALOUS HALL EFFECT

A. Symmetry of the Berry curvature in $\boldsymbol{k}$ space

The intrinsic AHC is expressed as the Berry curvature integrated over the Brillouin zone (BRZ) of one-electron bands below the Fermi level[33,34] such as:

$$\sigma_{\alpha\beta} = -\frac{e^2}{\hbar}\int \frac{d\boldsymbol{k}}{(2\pi)^3}\sum_n f(\varepsilon_n(\boldsymbol{k})-\mu)\Omega_{n,\alpha\beta}(\boldsymbol{k}) \ , \quad (1)$$

where n is the band index and α, β=x, y, z with $\alpha \neq \beta$. The Berry curvature for the AHC is defined as

$$\Omega_{n,\alpha\beta}(\boldsymbol{k}) = -2\mathrm{Im}\sum_{m\neq n}\frac{v_{nm,\alpha}(\boldsymbol{k})v_{mn,\beta}(\boldsymbol{k})}{[\varepsilon_m(\boldsymbol{k})-\varepsilon_n(\boldsymbol{k})]^2} \quad (2)$$

from the Kubo-formula[30,35]. In these equations, the $\varepsilon_n(\boldsymbol{k})$ is the eigenvalue and

$$v_{nm,\alpha}(\boldsymbol{k}) = \frac{1}{\hbar}\left\langle u_n(\boldsymbol{k})\left|\frac{\partial \hat{H}(\boldsymbol{k})}{\partial k_\alpha}\right|u_m(\boldsymbol{k})\right\rangle, \quad (3)$$

where $u_{n\boldsymbol{k}}$ is the periodic cell part of the Bloch states and $\hat{H}(\boldsymbol{k}) = e^{-i\boldsymbol{k}\cdot\boldsymbol{r}}\hat{H}e^{i\boldsymbol{k}\cdot\boldsymbol{r}}$. For the convenience of our discussions, we hereafter use the vector form notations for the AHC and Berry curvature, i.e. $\boldsymbol{\sigma} = (\sigma^x,\sigma^y,\sigma^z) \equiv (\sigma_{yz},\sigma_{zx},\sigma_{xy})$ and $\boldsymbol{\Omega}_n = (\Omega_n^x,\Omega_n^y,\Omega_n^z) \equiv (\Omega_{n,yz},\Omega_{n,zx},\Omega_{n,xy})$.

From Eq. (1), the appearance of the AHC, σ^α, is governed by the Berry curvature in $\boldsymbol{k}$ space, $\Omega^\alpha(\boldsymbol{k})$. Thus let us first discuss the symmetry of the Berry curvature in $\boldsymbol{k}$ space. The group velocity is expressed with the Berry phase correction as follows[36,37]:

$$\dot{\boldsymbol{r}} = \frac{1}{\hbar}\frac{\partial\varepsilon_n(\boldsymbol{k})}{\partial\boldsymbol{k}} - \dot{\boldsymbol{k}}\times\boldsymbol{\Omega}_n(\boldsymbol{k}) \ . \quad (4)$$

Transformation property of the Berry curvature with respect to the symmetry elements of magnetic space groups can be derived from this equation since the properties of $\varepsilon_n(\boldsymbol{k})$, $\dot{\boldsymbol{r}}$, $\boldsymbol{k}$ and $\dot{\boldsymbol{k}}$ are known. First, the Berry curvature is not modified by any translation operations. Second, it is transformed as ordinary vectors for rotation operations in $\boldsymbol{k}$ space. Third, the space inversion brings $\boldsymbol{\Omega}_n(\boldsymbol{k})$ to $\boldsymbol{\Omega}_n(-\boldsymbol{k})$. Thus the Berry curvature $\boldsymbol{\Omega}_n(\boldsymbol{k})$ behaves as an axial vector in $\boldsymbol{k}$ space. Finally, the time reversal operation transforms $\boldsymbol{\Omega}_n(\boldsymbol{k})$ to $-\boldsymbol{\Omega}_n(-\boldsymbol{k})$.

These transformation properties of the Berry curvature define constraints on its structure in $\boldsymbol{k}$ space. The well known relations are $\boldsymbol{\Omega}_n(-\boldsymbol{k}) = \boldsymbol{\Omega}_n(\boldsymbol{k})$ for systems with the space inversion symmetry and $\boldsymbol{\Omega}_n(-\boldsymbol{k}) = -\boldsymbol{\Omega}_n(\boldsymbol{k})$ for systems with the time reversal symmetry. Some of other relations are listed in Table I. These relations define further constraints on the Berry curvature at some $\boldsymbol{k}$ points, related to the elements of the group of $\boldsymbol{k}$. A simple example is that the Berry curvature is zero for all over the BRZ under both the space inversion and time reversal symmetries since the successive transformation of these operations results in $\boldsymbol{\Omega}_n(\boldsymbol{k}) = -\boldsymbol{\Omega}_n(\boldsymbol{k})$, leading to $\boldsymbol{\Omega}_n(\boldsymbol{k}) = 0$. Another example is the magnetic systems which have TC_{2z} symmetry. In this case, $\Omega^z(\boldsymbol{k}) = 0$ on the $k_z = 0$ plane since $\Omega^z(k_x,k_y,0) = -\Omega^z(k_x,k_y,0)$.

TABLE II. Complete list of symmetry operators and AHC components forbidden to be finite. The translation part of the operators, which does not affect the results, is not shown. In this table, all the superscripts of the AHC are explicitly written such as $\sigma_{ij}^{\ell} \equiv \sigma^{\ell} = \sigma_{ij}$ $(i,j,\ell = x,y,z)$. $C_{n(ij)}$ indicate the n-fold rotation operators whose rotation axes are in the (ij)-plane, $C_{n\mu}$ the n-fold rotation operators along the μ-axis. Mirror operator with the mirror plane normal to the μ-axis is $PC_{2\mu}$. The operator replacing the $C_{n\mu}$ to $C_{n\mu}^{-1}$ also belongs to the same category in the list. The integer in parenthesis shows the number of the O_h (D_{6h}) magnetic-point-group elements.

Cubic		
AHC component	Unitary	Anti unitary
σ_{ij}^{k}	$C_{n(ij)}$, $PC_{n(ij)}$ [n=2,4] (16)	TC_{nk}, TPC_{nk} [n=0,2,4] (16)
$\sigma^{[111]}$	$C_{2[1\bar{1}0]}$, $C_{2[01\bar{1}]}$, $C_{2[\bar{1}01]}$, $PC_{2[1\bar{1}0]}$, $PC_{2[01\bar{1}]}$, $PC_{2[\bar{1}01]}$ (6)	$TC_{n[111]}$, $TPC_{n[111]}$ [n=0,3] (6)
Hexagonal		
AHC component	Unitary	Anti unitary
σ_{xy}^{z}	$C_{2(xy)}$, $PC_{2(xy)}$ (12)	TC_{nz}, TPC_{nz} [n=0,2,3,6] (12)
σ_{yz}^{x}	C_{nz}, PC_{nz} [n=2,3,6]	TC_{nz}, TPC_{nz} [n=0,3,6]
	C_{2y}, PC_{2y} (12)	TC_{2x}, TPC_{2x} (12)
σ_{zx}^{y}	C_{nz}, PC_{nz} [n=2,3,6]	TC_{nz}, TPC_{nz} [n=0,3,6]
	C_{2x}, PC_{2x} (12)	TC_{2y},TPC_{2y} (12)

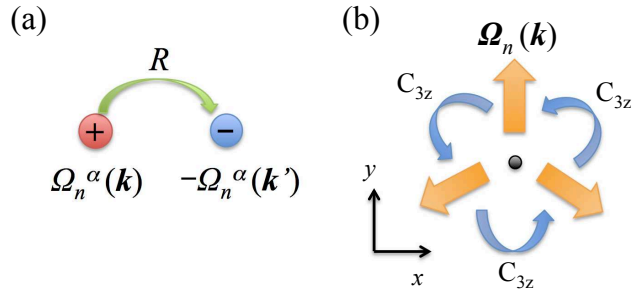

FIG. 1. Transformation of the Berry curvature under the symmetry operators. (a) Operators which reverse the sign of the Berry curvature and (b) the three-fold rotation along the z-axis.

B. Symmetry condition of finite AHC

From Eq. (1), the symmetry of the Berry curvature in $\boldsymbol{k}$ space, discussed in the previous subsection, determines whether σ^{α} can be finite or not in a magnetic system. Since the Berry curvature is not affected by any translation symmetries, it is enough to take only the magnetic point group into account. If the Berry curvature satisfies the condition $\Omega^{\alpha}(R\boldsymbol{k}) = -\Omega^{\alpha}(\boldsymbol{k})$ due to a magnetic symmetry, the corresponding AHC component σ^{α} must be zero since the Berry curvature at $\boldsymbol{k}$ and $R\boldsymbol{k}$ are canceled out by the BRZ integration (see Fig. 1 (a)). In this case, $\Omega^{\alpha}(\boldsymbol{k})$ is zero when R is an element of the group of $\boldsymbol{k}$, i.e. $R\boldsymbol{k} = \boldsymbol{k}$. Similarly, when a magnetic system has an n-fold rotation symmetry, the Berry curvature is canceled out through the BRZ integration in Eq. (1) (Fig. 1 (b)). The components of $\boldsymbol{\sigma}$ normal to the n-fold axis thus disappear. For example, σ^{x} and σ^{y} are zero when the system has a rotation symmetry with respect to the z-axis. We provide a complete list of the relation between the symmetry operators and the forbidden components of the AHC in Table II. The AHC component can be finite when the magnetic order breaks all of the corresponding symmetries listed in Table II. Structures of the AHC tensors under all the magnetic point-group symmetries have been listed in Refs. 18 and 19 by considering the transformation coefficients for the operators of magnetic point groups. Table II is equivalent to the lists in these previous works. Note that the symmetry operators in Table II also forbid finite magnetization M_{α}. This is because M_{α} and σ^{α} have the same transformation property for the magnetic symmetry operations, which is a natural consequence from the same transformation property of the Berry curvature and that of the magnetic moment in $\boldsymbol{k}$ space with respect to the operators of the magnetic space group.

C. S-O coupling and AHC

The effect of the S-O coupling on the AHE has been one of the fundamental issues since the pioneering work by Karplus and Luttinger[20]. Here, we provide a comprehensive explanation for the relation between the S-O coupling and the AHE in general magnetic states. First, let us note that the symmetry group for a non-magnetic system without the S-O coupling is expressed as $\mathcal{M}_{\rm nmag,nso} = \mathcal{M}_{\rm para} \times SU(2)$, where $\mathcal{M}_{\rm para} = \mathcal{G} \times \{E, T\}$, $\mathcal{G}$ is the ordinary space group of the crystal structure and E is the identity element of the space group. Magnetic order breaks both $\mathcal{M}_{\rm para}$ and $SU(2)$. However, in general, the symmetry of a magnetic system without the S-O coupling is higher than that with the S-O coupling by

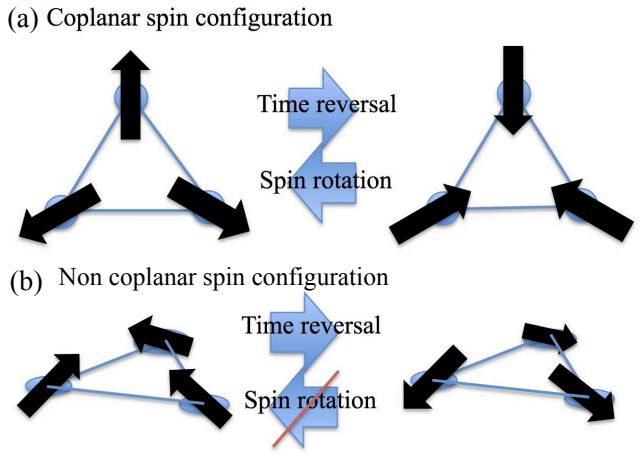

FIG. 2. Time reversal operation and global spin rotation for a (a) coplanar spin configuration and (b) non coplanar spin configuration in the triangular system.

the following reason. The symmetry group of a magnetic system without the S-O coupling, $\mathcal{M}_{\rm mag,nso}$, belongs to a subgroup of $\mathcal{M}_{\rm nmag,nso}$, and that with the S-O coupling, $\mathcal{M}_{\rm mag,so}$, belongs to a subgroup of $\mathcal{M}_{\rm para}$ because the S-O coupling breaks all of the symmetries related to $SU(2)$. Therefore, $\mathcal{M}_{\rm mag,so}$ is a subgroup of $\mathcal{M}_{\rm mag,nso}$. As discussed in section II A, the transformation property of the Berry curvature with respect to magnetic symmetry operations is similar to that of spin in $\boldsymbol{k}$ space, i.e. it is transformed as an axial vector and reversed by T. Meanwhile, the spin rotation $R_s(\theta_S, \phi_S)$ does not affect the Berry curvature in the absence of the S-O coupling. As a result, the magnetic symmetries listed in Table II preserved by further multiplying the spin rotations also forbid the corresponding σ^α to be finite in magnetic systems without the S-O coupling.

Ordinary collinear FM system is the most fundamental example in which the S-O coupling is required to induce the AHE. The FM systems without the S-O coupling always preserve the time reversal symmetry with the spin rotations $R_S(\theta_S, \phi_S)$. The $R_S T$ symmetry preserved in the system without the S-O coupling was referred as "effective T symmetry" in Ref. 31. Coplanar AFM spin configurations also require the S-O coupling to induce the AHE due to the $R_S T$ symmetry preserved in the absence of the S-O coupling, since T works as the 180-degrees-spin rotation around the axis normal to the coplanar plane [Fig. 2 (a)]. If the spin moments rise up from the coplanar plane, the spin configuration after operating T can not be brought back with the spin rotation R_S due to the spin components normal to the coplanar plane [Fig. 2 (b)]. In this case, the non-coplanar spin system breaks the $R_S T$ symmetry as well as T symmetry and the AHC therefore can be finite without the S-O coupling. This idea also explains why scalar spin chirality can induce the AHE[6], since finite scalar spin chirality always breaks the $R_S T$ symmetry.

Mn_3Ir, Mn_3Sn, and Mn_3Ge undergo coplanar magnetic order and require the S-O coupling to induce the AHE from the above discussions. Indeed, the first-principles calculation for Mn_3Ir confirmed that a finite spin component normal to the coplanar plane is required for finite AHC in the absence of the S-O coupling[12].

III. CLUSTER MULTIPOLE MOMENTS IN AFM STATES

A. Definition of CMP

As discussed in Sec. II B, magnetic structures induce finite AHC σ^α in the same symmetry condition for finite magnetization M_α in the presence of the S-O coupling. This means that the magnetic systems having net magnetization always belong to the symmetry which can induce the AHE with the S-O coupling. On the other hand, finite magnetization is not necessary to induce the AHE in AFM states. The question is then "is there a macroscopic order parameter which characterizes the AHE?". For identifying such an order parameter in generic magnetic states, we here introduce a quantity, which we call a cluster multipole moment (CMP). With the framework based on the CMP, we can quantify the symmetry breaking due to commensurate non-collinear magnetic order. Below, we provide general theory of the CMP. A concrete example is provided in Sec. III C for Mn_3Ir and Mn_3Z.

We first identify atom clusters for which we define the CMP moments. In general, a crystal contains a number of atoms which are inequivalent under the crystal symmetry. Each atom cluster is defined as a set of atoms related with one another by the *crystal* symmetry operators without space translation in the *magnetic* unit cell. For simplicity, we here consider only the case of the magnetic order characterized by the wave vector $\boldsymbol{q} = \boldsymbol{0}$, whose magnetic unit cell is the same with that of the crystal unit cell[38]. A space group $\mathcal{G}$, which describes the symmetry of a crystal structure, is decomposed into the cosets of the maximum symmorphic subgroup $\mathcal{H}$ as

$$\mathcal{G} = \sum_{i=1}^{N_{\rm coset}} \{R_i|\boldsymbol{\tau}_i\}\mathcal{H} \ , \tag{5}$$

where $N_{\rm coset}$ is the number of the cosets, R_i and $\boldsymbol{\tau}_i$ represent the point-group element and translation operator of the element in the space group $\mathcal{G}$, respectively, with $\{R_1|\boldsymbol{\tau}_1\} \equiv \{E|\boldsymbol{0}\}$ and $\boldsymbol{\tau}_i \neq \boldsymbol{0}$ for $i \geq 2$. In Eq. (5), $N_{\rm coset} = 1$ for crystal structures which belong to symmorphic space groups and $N_{\rm coset} > 1$ for crystal structures which belong to nonsymmorphic space groups. Therefore, nonsymmorphic crystal structures contain multiple clusters related with one another by the symmetry operators $\{R_i|\boldsymbol{\tau}_i\}$ in the unit cell. The origin of the cluster is naturally defined as the point which satisfies all the point symmetries for which the cluster is defined.

Analogous to the local multipole moments defined for an atom[24,25,27], here we define the rank-p CMP moment

for the μ-th cluster as follows:

$$M_{pq}^{(\mu)} \equiv \sqrt{\frac{4\pi}{2p+1}} \sum_{i=1}^{N_{\rm atom}^{(\mu)}} \boldsymbol{m}_i \cdot \nabla_i (|\boldsymbol{R}_i|^p Y_{pq}(\theta_i, \phi_i)^*) \ , (6)$$

where $N_{\rm atom}^{(\mu)}$ is the number of atoms of the μ-th cluster, $\boldsymbol{m}_i$ is a magnetic moment on the i-th atom, $\nabla_i \equiv \frac{\partial}{\partial \boldsymbol{R}_i}$, $\boldsymbol{R}_i \equiv (X_i, Y_i, Z_i)$ is the position of the i-th atom, Y_{pq} are the spherical harmonics, and R_i, θ_i and ϕ_i are the distance, polar angle and azimuthal angle, respectively, of the i-th atom. Based on the Wannier bases, $\{w_{i,a}\}$, the magnetic moment on the i-th atom is calculated as follows:

$$\boldsymbol{m}_i = \mu_B \sum_n \sum_{ab} \int \frac{d\boldsymbol{k}}{(2\pi)^3} f(\varepsilon_n(\boldsymbol{k}) - \mu) \times \langle u_n(\boldsymbol{k}) | w_{i,a} \rangle \langle w_{i,a} | (\boldsymbol{\ell} + 2\boldsymbol{s}) | w_{i,b} \rangle \langle w_{i,b} | u_n(\mathbf{k}) \rangle \ , \quad (7)$$

where $\mu_B = -|e|\hbar/2m$ is the Bohr magneton, and $\boldsymbol{\ell}$ and $\boldsymbol{s}$ are the orbital and spin angular momentum operators. The macroscopic contribution of the CMP moment can be defined by the summation over the clusters in the magnetic unit cell:

$$M_{pq} = \frac{N_{\rm atom}^{\rm u}}{N_{\rm atom}^{\rm c}} \frac{1}{V} \sum_{\mu=1}^{N_{\rm cluster}} M_{pq}^{(\mu)} \ , \quad (8)$$

where V is the volume of the magnetic unit cell, $N_{\rm atom}^{\rm u}$ is the number of atoms in the magnetic unit cell, $N_{\rm atom}^{\rm c} = \sum_\mu N_{\rm atom}^{(\mu)}$ is the total number of atoms in all of the clusters, and $N_{\rm cluster}$ is the number of clusters in the unit cell, which is the same with the multiplication of $N_{\rm coset}$ and the number of atoms inequivalent under the space-group symmetry.

B. Symmetry classification of CMP moments

The local multipole moments for f-electron systems are classified according to the irreducible representations (IREPs) of the point group symmetry of the atomic site[24,26,27,39–42]. Similarly, the CMP moments can be classified according to the point group symmetry of the atomic configuration. For a crystal structure whose conventional crystal axes are orthogonal, the CMP moments are classified according to the IREPs of the O_h point group in Table III. For a crystal structure with the hexagonal conventional axes such as the hexagonal and trigonal lattice systems, the CMP moments classified according to the D_{6h} IREPs should be used to reflect the point group symmetry. In Table IV, we provide a list of the D_{6h} CMP moments. These CMP moments are all odd with respect to the time reversal operator T. If the magnetic structure preserves the inversion symmetry, only odd rank CMP moments can be finite due to the relation $M_{pq} = (-)^{p+1} M_{pq}$ in Eq. (6). Figure 3 shows non-collinear magnetic structures characterized by the lowest rank cluster octupole moments for the D_{6h} IREPs.

Ordinary magnetization M_α ($\alpha = x, y, z$) corresponds to the macroscopic contribution of the cluster dipole moment J_α. Meanwhile, magnetization of non-collinear AFM states without net dipole magnetization is characterized by the macroscopic contribution of CMP moments with the ranks higher than one. From the discussion of Sec. II B, σ^α, M_α, and J_α are transformed in the same manner for the operation of the magnetic-point-group elements, which means that they belong to the same IREPs of the O_h and D_{6h} point groups. The conditions for the AHE can now be concisely described with the symmetrized CMP moments. The AHE is induced with the emergence of the finite magnetization of the CMP moments which belong to the same IREP of dipole moments, i.e. T_{1g} (A_{2g} and/or E_{1g}) CMP moments in the $O_h(D_{6h})$ representation. Note that, in the absence of the S-O coupling, the AHE requires $R_s T$-symmetry breaking as well as magnetization of these CMP moments as discussed in Sec. II C.

C. CMP moment and AHE in Mn_3Ir and Mn_3Z

Let us now apply the scheme discussed above to the AFM spin configurations observed in Mn_3Ir and Mn_3Z, for which the AHE in the AFM states has been stud-

TABLE III. CMP moments up to rank three classified according to the IREPs of the O_h point group. The quadrupole CMP moments can be finite only for magnetic structures without the space inversion symmetry (see text). Note that this table is analogous to the *magnetic* multipole moments classified according to the O_h point group, and the similar list is provided for electric multipole moments in Ref. 39.

	IREP	CMP
Rank 1	T_{1g}	$J_x \equiv \frac{1}{\sqrt{2}}(-M_{11}+M_{1-1})$
(Dipole)		$J_y \equiv -\frac{i}{\sqrt{2}}(M_{11}+M_{1-1})$
		$J_z \equiv M_{10}$
Rank 2	E_u	$Q_{3z^2-r^2} \equiv M_{20}$
(Quadrupole)		$Q_{x^2-y^2} \equiv \frac{1}{\sqrt{2}}(M_{22}+M_{2-2})$
	T_{2u}	$Q_{yz} \equiv -\frac{i}{\sqrt{2}}(M_{21}+M_{2-1})$
		$Q_{zx} \equiv \frac{1}{\sqrt{2}}(-M_{21}+M_{2-1})$
		$Q_{xy} \equiv \frac{i}{\sqrt{2}}(M_{22}-M_{2-2})$
Rank 3	A_{2g}	$T_{xyz} \equiv \frac{i}{\sqrt{2}}(M_{32}-M_{3-2})$
(Octupole)	T_{1g}	$T_x^\alpha \equiv \frac{1}{4}[\sqrt{5}(-M_{33}+M_{3-3})-\sqrt{3}(-M_{31}+M_{3-1})]$
		$T_y^\alpha \equiv \frac{i}{4}[\sqrt{5}(M_{33}+M_{3-3})+\sqrt{3}(M_{31}+M_{3-1})]$
		$T_z^\alpha \equiv M_{30}$
	T_{2g}	$T_x^\beta \equiv -\frac{1}{4}[\sqrt{3}(-M_{33}+M_{3-3})+\sqrt{5}(-M_{31}+M_{3-1})]$
		$T_y^\beta \equiv \frac{i}{4}[\sqrt{3}(M_{33}+M_{3-3})-\sqrt{5}(M_{31}+M_{3-1})$
		$T_z^\beta \equiv \frac{1}{\sqrt{2}}(M_{32}+M_{3-2})$

TABLE IV. CMP moments up to rank three classified according to the IREPs of the D_{6h} point group. Note that this table is analogous to the *magnetic* multipole moments classified according to the D_{6h} point group. The quadrupole CMP moments can be finite only for magnetic structures without the space inversion symmetry (see text).

	IREP	CMP
Rank 1	A_{2g}	$J_z \equiv M_{10}$
(Dipole)	E_{1g}	$J_x \equiv \frac{1}{\sqrt{2}}(-M_{11}+M_{1-1})$
		$J_y \equiv -\frac{i}{\sqrt{2}}(M_{11}+M_{1-1})$
Rank 2	A_{1u}	$Q_{3z^2-r^2} \equiv M_{20}$
(Quadrupole)	E_{2u}	$Q_{x^2-y^2} \equiv \frac{1}{\sqrt{2}}(M_{22}+M_{2-2})$
		$Q_{xy} \equiv \frac{i}{\sqrt{2}}(M_{22}-M_{2-2})$
	E_{1u}	$Q_{zx} \equiv \frac{1}{\sqrt{2}}(-M_{21}+M_{2-1})$
		$Q_{yz} \equiv -\frac{i}{\sqrt{2}}(M_{21}+M_{2-1})$
Rank 3	A_{2g}	$T_z^\alpha \equiv M_{30}$
(Octupole)	E_{1g}	$T_x^\gamma \equiv \frac{1}{\sqrt{2}}(-M_{31}+M_{3-1})$
		$T_y^\gamma \equiv -\frac{i}{\sqrt{2}}(M_{31}+M_{3-1})$
	E_{2g}	$T_{xyz} \equiv \frac{i}{\sqrt{2}}(M_{32}-M_{3-2})$
		$T_z^\beta \equiv \frac{1}{\sqrt{2}}(M_{32}+M_{3-2})$
	B_{2g}	$T_x^\zeta \equiv \frac{1}{\sqrt{2}}(-M_{33}+M_{3-3})$
	B_{1g}	$T_y^\zeta \equiv \frac{i}{\sqrt{2}}(M_{33}+M_{3-3})$

ied[12,14–16]. Mn_3Ir crystallizes into the simple cubic structure which belongs to the space group $Pm\overline{3}m$ (O_h^1, No. 221) as shown in Fig. 4. This crystal structure leads to $N_{\rm coset}=1$ in Eq. (5) since the space group is symmorphic. Here, we focus on the Mn atoms, which have the finite magnetic moments in the AFM state. The unit cell contains three Mn atoms ($N^u_{\rm atom}$=3), and we can define a Mn cluster, which contain six Mn atoms ($N^c_{\rm atom}$=6) related to each other with the operation of the symmetry elements of the O_h point group. In Fig. 4 (b), we show the AFM structures characterized by T_{1g} octupole moment with the order parameter T_x^α=T_y^α=T_z^α, which has been recognized experimentally, and T_{2g} octupole moment with T_x^α=T_y^α=T_z^α. Following the discussion in Sec. III B, the AFM configuration with T_{1g} cluster octupole moments, which belong to the same IREP of the dipole moment, can induce the AHE, as predicted in the earlier work by first-principles calculation[12], while that with T_{2g} does not. The crystal symmetries broken by the T_{1g} cluster octupole moment are completely the same as those broken by the co-linear magnetic dipole order along a [111] direction. As a result, the magnetic space group ($R\overline{3}m'$) for the AFM state with the T_{1g} CMP, whose symmetry elements are listed in Table V, is in common with the FM state.

Mn_3Z crystallizes into the Ni_3Sn-type structure as shown in Fig. 5 (a). The hexagonal structure of Mn_3Z belongs to the space group $P6_3/mmc$ (D^4_{6h}, space

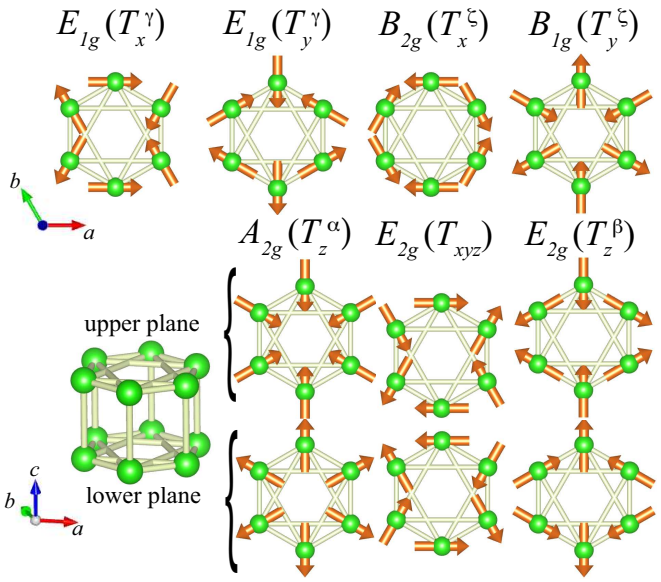

FIG. 3. AFM structures characterized by the cluster octupole moments of the D_{6h} IREPs in Table IV.

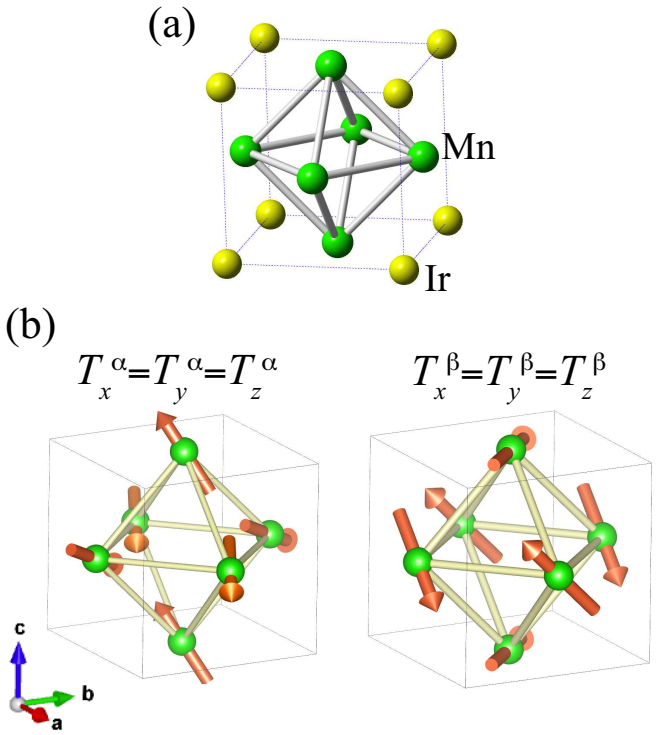

FIG. 4. (a) Crystal structure of Mn_3Ir. (b) The AFM structures characterized by the cluster octupole moments of T_{1g} CMP with the relation $T_x^{\alpha}=T_y^{\alpha}=T_z^{\alpha}$, which has been recognized experimentally, and of T_{2g} CMP with $T_x^{\beta}=T_y^{\beta}=T_z^{\beta}$ in the Mn cluster of Mn_3Ir.

group No. 194)[43,44]. The nonsymmorphic space group $P6_3/mmc$ is decomposed into the cosets of the symmorphic space group $P\bar{3}m1$ (D_{3d}^3, No. 164) as $P6_3/mmc = P\bar{3}m1 + \{C_{2z}|\boldsymbol{\tau}\}P\bar{3}m1$ ($D_{3d}^3 + \{C_{2z}|\boldsymbol{\tau}\}D_{3d}^3$), where $\boldsymbol{\tau} = (0, 0, c/2)$. Following the discussion of Sec. III, Mn_3Z contains four clusters, i.e. two clusters related to each other with the operation of $\{C_{2z}|\boldsymbol{\tau}\}$ for Mn and Z atoms in the magnetic unit cell (see Fig. 5 (a)). Each cluster has the point group symmetry of D_{3d}. Since the magnetic moments in Z atoms are negligible, we here ignore the Z-atom clusters. The macroscopic contribution of the CMP moment is calculated from Eq. (8) with $N_{\rm atom}^{\rm u}/N_{\rm atom}^{\rm c} = 1/2$, since the unit cell of Mn_3Z contains six Mn-atoms ($N_{\rm atom}^{\rm u} = 6$) and two Mn clusters consist of six Mn atoms for each cluster ($N_{\rm atom}^{\rm c} = 12$) as shown in Fig. 5 (a). The D_{3d} point group has six IREPs $A'_{1g/u}$, $A'_{2g/u}$, $E'_{g/u}$ in which the prime is for distinguishing the IREPs from those of the D_{6h} point group. The compatibility relations between the D_{3d} and D_{6h} IREPs are as follows:

$$A_{1g/u} \downarrow D_{3d} = B_{2g/u} \downarrow D_{3d} = A'_{1g/u}$$
$$A_{2g/u} \downarrow D_{3d} = B_{1g/u} \downarrow D_{3d} = A'_{2g/u}$$
$$E_{1g/u} \downarrow D_{3d} = E_{2g/u} \downarrow D_{3d} = E'_{g/u} \ .$$

These relations mean, for instance, A_{1g} and B_{2g} CMP moments belong to the same IREP, A'_{1g}, in the cluster with the D_{3d} point group symmetry.

Next, we identify the CMP moments which characterize the AFM states of Mn_3Z. We here mainly focus on the AFM states of Mn_3Sn, whose magnetic structures have been well established experimentally[44–46]. Mn magnetic moments in Mn_3Sn form the so-called inverse triangular spin structure below the Néel temperature of $T_{\rm N1} \simeq$420K[44,45] (Fig. 5 (b)). Mn_3Sn undergoes another phase transition at $T_{\rm N2} \sim$50K but the detailed magnetic structure for the low temperature phase is unknown. We therefore focus on the magnetic phase above 50K. Interestingly, the inverse triangular spin structure rotates following the direction of applied magnetic fields in the

TABLE V. Magnetic symmetry operators preserved in the AFM states of Mn_3Ir and Mn_3Sn. In Mn_3Ir, the directions of the rotation axes are expressed with the cubic (Cartesian) axis. In Mn_3Sn, the x,y axes are shown in Fig. 5 (b) and the z axis is the normal direction of the xy plane. $\boldsymbol{\tau}$ represents the translation (0, 0, c/2).

Spin struct.	Preserved Symmetries
Mn_3Ir	$\{E \mid \mathbf{0}\}, \{C_{3[111]}^{+} \mid \mathbf{0}\}, \{C_{3[111]}^{-} \mid \mathbf{0}\},$ $T\{C_{2[1\bar{1}0]} \mid \mathbf{0}\}, T\{C_{2[01\bar{1}]} \mid \mathbf{0}\}, T\{C_{2[\bar{1}01]} \mid \mathbf{0}\}$ $\{P \mid \mathbf{0}\}, \{PC_{3[111]}^{+} \mid \mathbf{0}\}, \{PC_{3[111]}^{-} \mid \mathbf{0}\},$ $T\{PC_{2[1\bar{1}0]} \mid \mathbf{0}\}, T\{PC_{2[01\bar{1}]} \mid \mathbf{0}\}, T\{PC_{2[\bar{1}01]} \mid \mathbf{0}\}$
Mn_3Sn AFM1	$\{E \mid \mathbf{0}\}, \{C_{2x} \mid \mathbf{0}\}, T\{C_{2z} \mid \boldsymbol{\tau}\}, T\{C_{2y} \mid \boldsymbol{\tau}\},$ $\{P \mid \mathbf{0}\}, \{PC_{2x} \mid \mathbf{0}\}, T\{PC_{2z} \mid \boldsymbol{\tau}\}, T\{PC_{2y} \mid \boldsymbol{\tau}\}$
Mn_3Sn AFM2	$\{E \mid \mathbf{0}\}, \{C_{2y} \mid \boldsymbol{\tau}\}, T\{C_{2z} \mid \boldsymbol{\tau}\}, T\{C_{2x} \mid \mathbf{0}\},$ $\{P \mid \mathbf{0}\}, \{PC_{2y} \mid \boldsymbol{\tau}\}, T\{PC_{2z} \mid \boldsymbol{\tau}\}, T\{PC_{2x} \mid \mathbf{0}\}$

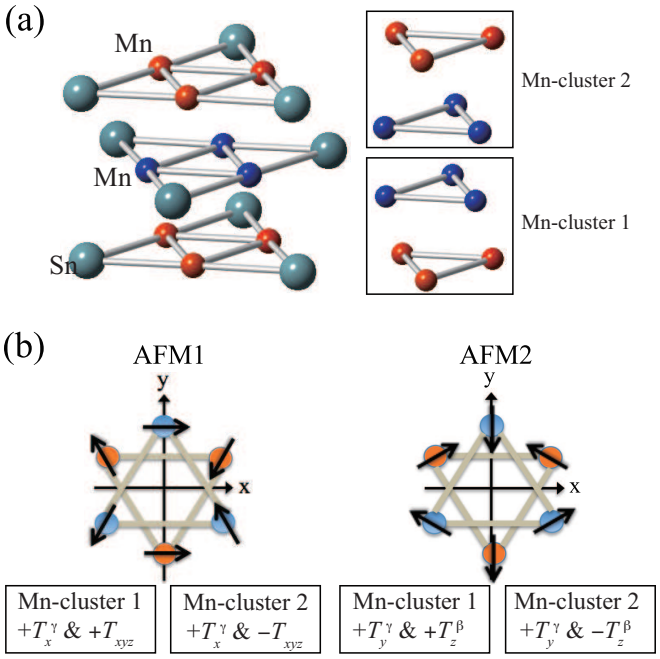

FIG. 5. (a) Crystal structure of Mn_3Z (Z=Sn, Ge) with the Mn-clusters defined by the space group (see text). (b) Spin configuration on the Mn atoms in Mn_3Sn. The AFM1 and AFM2 spin structures are experimentally realized depending on the direction of magnetic fields along the x and y directions, respectively[45]. The lowest rank CMP moments characterizing the spin configurations are also shown for each Mn-cluster.

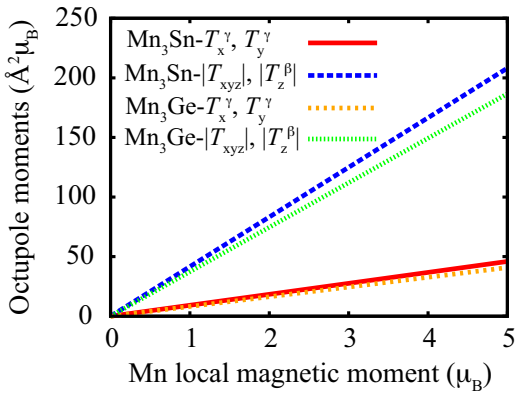

FIG. 6. Local-magnetic-moment dependence of the cluster octupole moments for the Mn-clusters in Mn_3Sn and Mn_3Ge. The parameters for the crystal structures are described in Sec. IV A. T_x^γ and T_{xyz} (T_y^γ and T_z^β) are for the AFM1 (AFM2) in Fig. 5.

c-plane[46]. We refer the magnetic structures under the magnetic fields along the x and y directions as AFM1 and AFM2, respectively, as shown in Fig. 5 (b). The magnetic space groups of the AFM1 and AFM2 magnetic structures belong to $Cmc'm'$ and $Cm'cm'$, respectively, taking the primary, secondary, and tertiary direction as the x, y, and z axes. The symmetry operators in the magnetic space group are listed in Table V. The magnetic space groups for AFM1 and AFM2 states are the same as those of the FM states with the magnetic moments along the x and y directions, respectively. Furthermore, these AFM states require the S-O coupling, as well as FM states, to induce the AHE from the discussion in Sec. II C on the coplanar spin configuration.

Because of the geometry of the magnetic alignments on the Mn atoms, there is no magnetization of the dipole moment if all the atoms have the same size of local magnetic moment[47]. Also, since the magnetic structures preserve the inversion symmetry, only the odd rank CMP moments are finite. Indeed, the CMP moments calculated for the AFM states with Eq. (6) are finite only for the odd ranks higher than one. The lowest rank CMP moments characterizing the AFM spin configurations are thus cluster octupole moments.

For the symmetry operators in the D_{3d} point group, the AFM1 (AFM2) magnetic configuration of Mn_3Sn has the same transformation property with the magnetic structure characterized by T_x^γ and T_{xyz} (T_y^γ and T_z^β) in Fig. 3. Namely, the magnetic modulation of AFM1 (AFM2) parallel to the xy-plane is characterized by T_x^γ (T_y^γ), and the three dimensional configuration is characterized by the T_{xyz} (T_z^β). The magnetic configurations in the different clusters are related to each other with the operation of TC_{2z} (See Table V and Fig. 5). The operation of TC_{2z} preserves T_x^γ (T_y^γ) and flips the sign of T_{xyz} (T_z^β) due to the transformation property for each IREP. As a result, T_x^γ and T_{xyz} (T_y^γ and T_z^β) octupole moments have ferro and antiferro alignments, respectively, between the neighboring clusters. Therefore, only the T_x^γ (T_y^γ)-octupole moment can have macroscopic magnetization in the AFM1 (AFM2) state.

In Fig. 6, we show how the cluster octupole moments in Mn_3Sn and Mn_3Ge change as a function of the local magnetic moment[48]. Here we assumed that all the Mn sites always have the same size of the local magnetic moment and Mn_3Ge has the same spin configurations with those of Mn_3Sn. In this situation, we can show from Eq. (6) that the octupole moments are proportional to the local magnetic moments. Thus the local moment can also quantify the symmetry breaking associated with the AHE. The local magnetic moment, however, cannot characterize general AFM orders when inequivalent magnetic atoms have different sizes of local moments. On the other hand, even in such cases, the CMP moments work as the order parameter quantifying the symmetry breaking.

IV. FIRST-PRINCIPLES ANALYSIS OF ANOMALOUS HALL EFFECT

A. Method

We performed the first-principles calculations for the AFM1 and AFM2 states of Mn_3Z (Z=Sn, Ge) with the QUANTUM ESPRESSO package[49] with the rela-

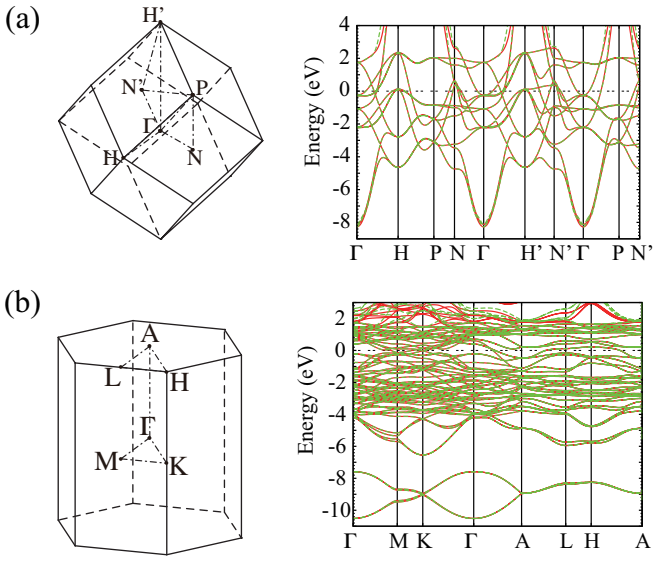

FIG. 7. BRZ and the energy bands for (a) the FM state of bcc-Fe and (b) the AFM1 state of Mn_3Sn. The red and green lines are the energy bands obtained from the first-principles calculations and from the Wannier interpolation, respectively.

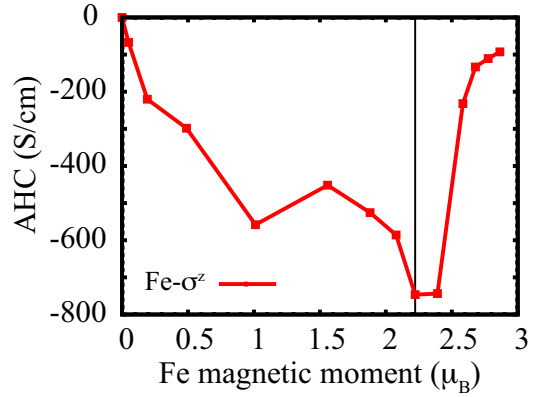

FIG. 8. Local magnetic moment (cluster dipole moment) dependence of the AHC in the FM states of bcc-Fe. The solid line in the plot indicates the local magnetic moment obtained by the first-principles calculation.

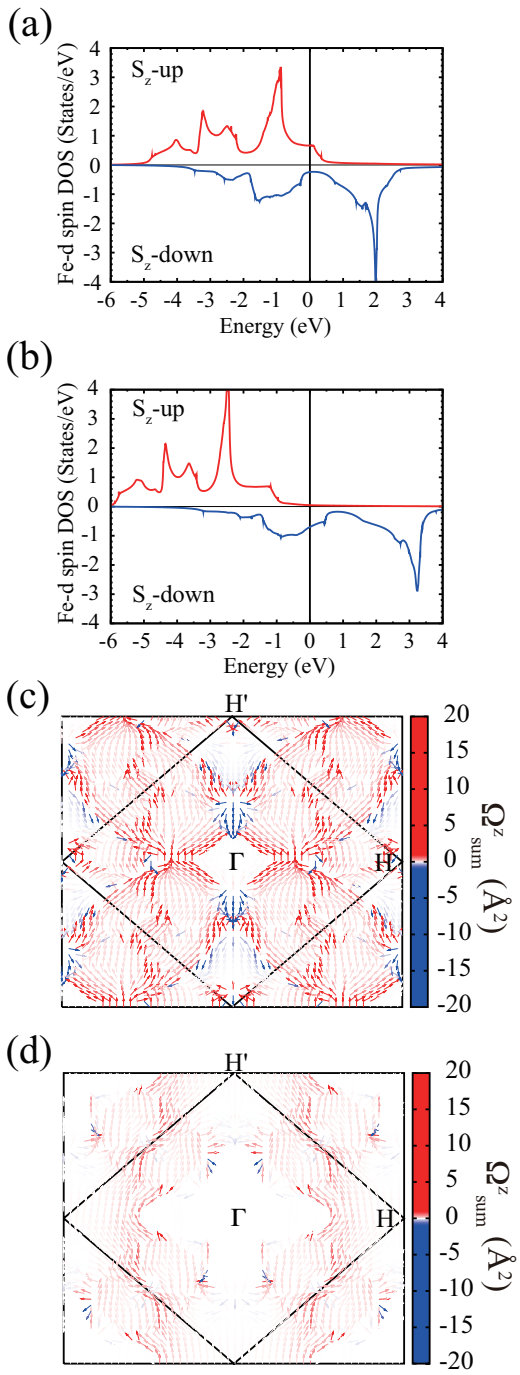

FIG. 9. Fe-d spin-projected DOS for the FM states of bcc-Fe with the magnetic moments (a) 2.22 μ_B and (b) 2.86 μ_B corresponding to λ= 1.0, and 2.0, respectively. (c) and (d) show $\boldsymbol{\Omega}_{\rm sum}(\boldsymbol{k})$ (see text) on the $k_y = 0$ plane corresponding to the states of (a) and (b), respectively. $\boldsymbol{\Omega}_{\rm sum}$ vectors are colored by the weight of $\Omega^z_{\rm sum}$, which contribute to the AHC.

tivistic version of the ultrasoft pseudo potentials using the exchange-correlation functional of the generalized gradient approximation (GGA) proposed by Perdew, Burke, and Ernzerhof[50]. We used the lattice constants a=5.665Å, c=4.531Å and the Wyckoff position of the Mn 6h atomic sites x=0.8388 from the experimental results[43,44]. For Mn_3Ge, the lattice constants a=5.34Å, c=4.31Å from the experiment were adopted[15] and the Wyckoff parameter of the Mn 6h atomic sites was taken the same as that of Mn_3Sn. The spin configuration was set such as Fig. 5 (b) for the AFM1 and AFM2 spin configurations. In the GGA calculations, we obtained the local magnetic moment 3.39μ_B for Mn_3Sn and 2.92μ_B for Mn_3Ge both for the AFM1 and AFM2 states. The calculations were performed also for bcc Fe as a reference FM system. The lattice constant 2.87Å was used. The spin moment was set to the $+z$ direction. The magnetic moment obtained from the GGA calculation is 2.22μ_B.

The realistic tight-binding models were obtained from

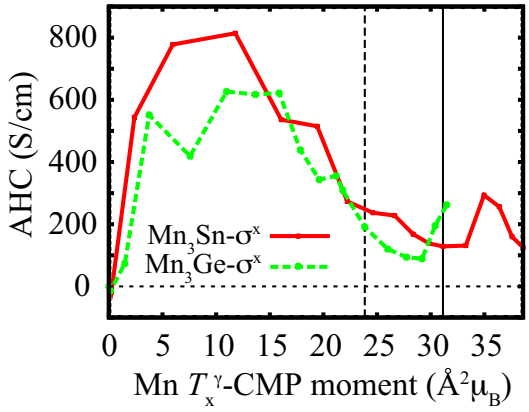

FIG. 10. Mn cluster T_x^γ-octupole moment dependence of the AHC in AFM1 states of Mn_3Sn and Mn_3Ge. The solid and dashed lines in the plot indicate the local magnetic moments obtained by the first-principles calculations for Mn_3Sn and Mn_3Ge, respectively, obtained by the first-principles calculations.

the first-principles band structures, using the Wannier90 program code[51]. The tight-binding model for bcc Fe was generated with the 18 orbitals of Fe-s, p, d orbitals, and Mn_3Z with the 88 orbitals using Mn-s, d and Z-s, p orbitals. The energy band structures of the tight-binding models show good agreement with those of the first-principles calculations as shown in Fig. 7. The Berry curvature and AHC were calculated within the tight-binding models with Eqs. (1), (2) and (3).

To discuss the magnetic-moment dependence of the AHC, we also performed the calculations for nonmagnetic states with the S-O coupling and obtained the tight-binding Hamiltonian $H_{\rm nmag}$ as well as the Hamiltonian for the magnetic state with the S-O coupling, $H_{\rm mag}$. We further generated the hopping matrices obtained by interpolating or extrapolating these tight-binding Hamiltonian matrices such as $H_\lambda = H_{\rm nmag} + \lambda(H_{\rm mag} - H_{\rm nmag})$ ($\lambda \geq 0$). The Fermi level was determined so as to preserve the electron number for each H_λ, and then the AHC was calculated for the obtained electronic structure and the Fermi level.

B. Ferromagnetic states of bcc Fe

Before proceeding to the first-principles analysis of the AFM states of Mn_3Z, we discuss the AHE in the FM states of bcc Fe, which has well been investigated theoretically[30–32,52]. Figure 8 shows the magnetic moment (cluster dipole moment) dependence of the AHC for bcc Fe. The AHC increases as the magnetic moment increases in the small magnetic moment region and makes a peak around $2.22\mu_B$ obtained in the GGA calculation, and then decreases. Figures 9 (a) and (b) show spin density of states (DOS) of the Fe-d orbitals for the electronic structures with the magnetic moments $2.22\mu_B$, and $2.86\mu_B$, respectively. The original magnetic state

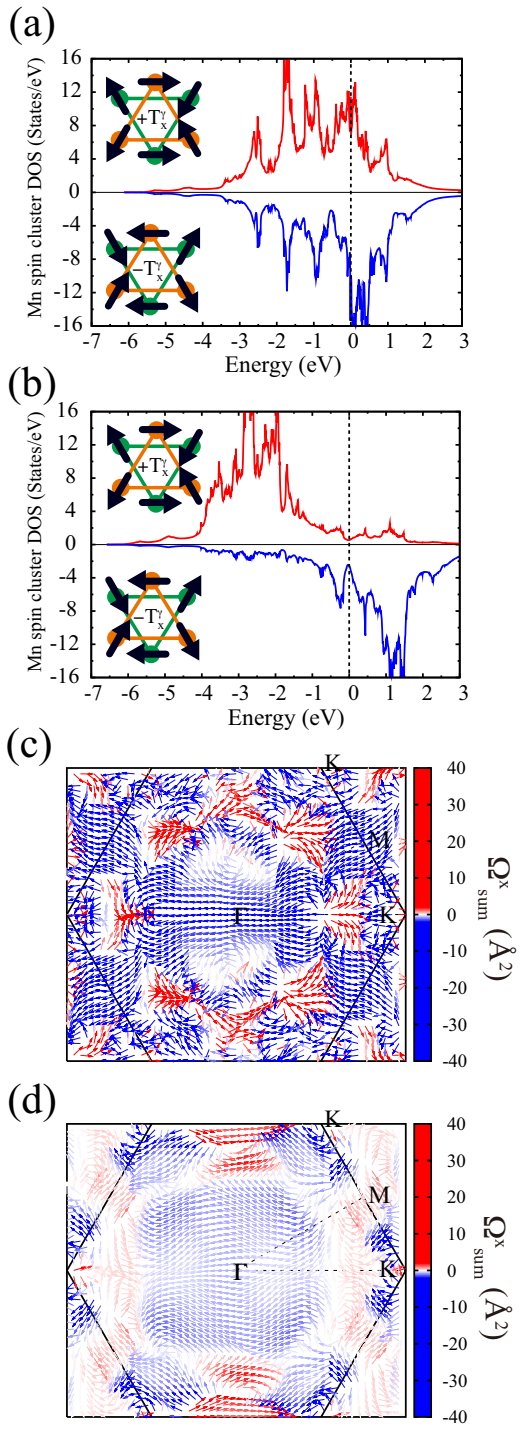

FIG. 11. Projected DOS for the AFM states of Mn_3Sn with the Mn T_x^γ-CMP (local magnetic moment) (a) $11.8\text{Å}^2\mu_B$ ($1.28\mu_B$) and (b) $31.2\text{Å}^2\mu_B$ ($3.39\mu_B$) corresponding to λ=0.20, 1.0, respectively. (c) and (d) show $\boldsymbol{\Omega}_{\rm sum}(\boldsymbol{k})$ (see text) on the $k_z = 0$ plane corresponding to the states of (a) and (b), respectively. $\boldsymbol{\Omega}_{\rm sum}$ vectors are colored by the weight of $\Omega^x_{\rm sum}$, which contribute to the AHC.

with the magnetic moment $2.22\mu_B$ has the contribution from both the majority- (up-) and minority- (down-)spin DOS at the Fermi level. Meanwhile, the DOS of Fig. 9 (b) shows that the up-spin states are almost fully occupied due to the large spin moment and do not have weight at the Fermi level. Figures 9 (c) and (d) show the $\boldsymbol{k}$-dependence of the Berry curvature summed over the occupied states, $\boldsymbol{\Omega}_{\rm sum}(\boldsymbol{k}) = \sum_n f(\varepsilon_n(\boldsymbol{k}) - \mu)\boldsymbol{\Omega}_n(\boldsymbol{k})$, on the $k_y = 0$ plane. In both states, $\Omega^z_{\rm sum}$ is positive in a large region of the BRZ, leading to negative σ^z by the BRZ integration. Meanwhile, we see that the intensity of $\Omega^z_{\rm sum}(\boldsymbol{k})$ is much stronger in Fig. 9 (c) than in Fig. 9 (d).

C. Antiferromagnetic states of Mn_3Sn

Let us move on to Mn_3Z. We here mainly focus on the AFM1 state of Mn_3Sn, whose crystal and magnetic structures have been well established experimentally[44–46]. The local Mn magnetic moment $3.39\mu_B$ and σ_{yz}=129(S/cm) obtained from the GGA calculation agree well with the experimental measurement of the local magnetic moment $3\mu_B$ and that of the AHC $\sim$100(S/cm)[14]. The calculated value is also consistent with a recent work[23]. Figure 10 shows that the AHC in Mn_3Sn and Mn_3Ge shows a similar CMP-moment dependence. The calculations also show that decreasing the magnetic moments from the one obtained with GGA makes the size of the AHC larger. In fact, for the electronic structure obtained by the GGA calculation, the AHC (magnetization) of Mn_3Ge is larger (smaller) than that of Mn_3Sn. This is consistent with the recent experiments[14–16].

For the AFM states of Mn_3Sn, we define the Mn cluster spin bases as the two symmetrized spin configurations related by the time reversal symmetry (see the insets of Fig. 11 (a) and (b)). The two spin configurations are characterized by the positive and negative T^γ_x octupole moments. Then, we can discuss the AHE in terms of the spin cluster, in analogy with the majority- and minority-spin states in the FM systems. Figures 11 (a) and (b) show the projected DOS for each spin cluster corresponding to the T^γ_x= 11.8Å$^2\mu_B$ and 31.2Å$^2\mu_B$, respectively. The magnetic state with T^γ_x=11.8Å$^2\mu_B$ has a large DOS contribution from the both spin cluster components at the Fermi level. On the other hand, in the magnetic state with the large T^γ_x moment, the spin cluster states characterized by the positive T^γ_x are almost fully occupied due to the large octupole moment and only have small weight at the Fermi level. Figures 11 (c) and (d) show $\boldsymbol{\Omega}_{\rm sum}(\boldsymbol{k})$ colored by the $\Omega^x_{\rm sum}$ component on the $k_z = 0$ plane. In both states, $\Omega^x_{\rm sum}$ is negative in a large region of the BRZ, leading to positive σ^x by the BRZ integration. The intensity of $\Omega^x_{\rm sum}(\boldsymbol{k})$ is stronger in Fig. 11 (c) than in Fig. 11 (d), which is a situation similar to that in Fig. 9 (c) and (d).

V. SUMMARY

We showed that the symmetry breaking due to the commensurate non-collinear magnetic order can be measured with the CMP moment, which is defined for atomic clusters in the crystal. We identified the degree of freedom responsible for the AHE in generic magnetic systems as the macroscopic contribution of T_{1g} (A_{2g} or/and E_{1g}) CMP moments for the O_h (D_{6h}) point-group representation. The theoretical framework was applied to the AFM states of Mn_3Ir and Mn_3Z. The AFM1 (AFM2) state of Mn_3Sn is characterized with the T^γ_x and T_{xyz} (T^γ_y and T^β_z) cluster octupole moments in the D_{6h} IREPs and the AHE is induced by the macroscopic contribution of T^γ_x (T^γ_y) with the S-O coupling. The AHC in the FM states of bcc-Fe and that in the AFM states of Mn_3Sn show similar dependence on the CMP moments. Thus, the CMP makes it possible to discuss the FM and AFM states in the same framework, and is useful to search for another new functional material having a large AHE.

ACKNOWLEDGMENTS

We thank S. Nakatsuji, H. Kusunose, and T. Miyake for helpful comments and discussions. This work was supported by JSPS KAKENHI Grant Numbers JP15K17713, JP15H05883 (J-Physics), JP16H04021, JP16H00924, JP16H06345 and PRESTO and CREST, Japan Science and Technology Agency.

[1] N. Nagaosa, J. Sinova, S. Onoda, A. MacDonald, and N. Ong, Rev. Mod. Phys. **82**, 1539 (2010).
[2] D. Xiao, M.-C. Chang, and Q. Niu, Rev. Mod. Phys. **82**, 1959 (2010).
[3] M. Gradhand, D. V. Fedorov, F. Pientka, P. Zahn, I. Mertig, and B. L. Gyrffy, J. Phys.: Condens. Matter **24**, 213202 (2012).
[4] S. Yoshii, S. Iikubo, T. Kageyama, K. Oda, Y. Kondo, K. Murata, and M. Sato, J. Phys. Soc. Jpn. **69**, 3777 (2000).
[5] Y. Taguchi, Y. Oohara, H. Yochizawa, N. Nagaosa, and Y. Tokura, Science **291**, 2573 (Mar 2001).
[6] R. Shindou and N. Nagaosa, Phys. Rev. Lett. **87**, 116801 (2001).
[7] S. Yoshii, S. Iikubo, T. Kageyama, K. Oda, Y. Kondo, K. Murata, and M. Sato, J. Phys. Soc. Jpn. **69**, 3777 (2006).
[8] T. Tomizawa and H. Kontani, Phys. Rev. B **80**, 100401 (2009).

[9] T. Tomizawa and H. Kontani, Phys. Rev. B **82**, 104412 (Sep 2010).
[10] Y. Taguchi, T. Sasaki, S. Awaji, Y. Iwasa, T. Tayama, T. Sakakibara, S. Iguchi, T. Ito, and Y. Tokura, Phys. Rev. Lett. **90**, 257202 (2003).
[11] Y. Taguchi, Y. Oohara, H. Yoshizawa, N. Nagaosa, T. Sasaki, S. Awaji, Y. Iwasa, T. Tayama, T. Sakakibara, S. Iguchi, *et al.*, J. Phys.: Condens. Matter **16**, S599 (2004).
[12] H. Chen, Q. Niu, and A. H. MacDonald, Phys. Rev. Lett. **112**, 017205 (2014).
[13] J. Kübler and C. Felser, Europhys. Lett. **108**, 67001 (2014).
[14] S. Nakatsuji, N. Kiyohara, and T. Higo, Nature **527**, 212 (2015).
[15] N. Kiyohara, T. Tomita, and S. Nakatsuji, Phys. Rev. Applied **5**, 064009 (2016).
[16] A. K. Nayak, J. E. Fischer, Y. Sun, B. Yan, J. Karel, A. C. Komarek, C. Shekhar, N. Kumar, W. Schnelle, J. Kübler, *et al.*, Sci. Adv. **2**, e1501870 (2016).
[17] H. Yang, Y. Sun, Y. Zhang, W.-J. Shi, S. S. P. Parkin, and B. Yan, arXiv:1608.03404 (2016).
[18] W. Kleiner, Phys. Rev. **142**, 318 (1966).
[19] M. Seemann, D. Ködderitzsch, S. Wimmer, and H. Ebert, Phys. Rev. B **92**, 155138 (2015).
[20] R. Karplus and J. Luttinger, Phys. Rev. **95**, 1154 (1954).
[21] It has been proposed that the scalar spin chirality can induce the AHE also in the spin liquid state. See e.g., Y. Machida, S. Nakatsuji, S. Onoda, T. Tayama, and T. Sakakibara, Nature 463, 210 (2010).
[22] N. Nagaosa and Y. Tokura, Nat. Nanotechnol. **8**, 899 (2013).
[23] Y. Zhang, Y. Sun, H. Yang, J. Železný, S. S. P. Parkin, C. Felser, and B. Yan, arXiv:1610.04034 (2016).
[24] H. Kusunose, J. Phys. Soc. Jpn. **77**, 064710 (2008).
[25] Y. Kuramoto, Prog. Theor. Phys. Suppl. **176**, 77 (2008).
[26] Y. Kuramoto, H. Kusunose, and A. Kiss, J. Phys. Soc. Jpn. **78**, 072001 (2009).
[27] P. Santini, S. Carretta, G. Amoretti, R. Caciuffo, N. Magnani, and G. H. Lander, Rev. Mod. Phys. **81**, 807 (2009).
[28] M.-T. Suzuki, N. Magnani, and P. M. Oppeneer, Phys. Rev. B **82**, 241103 (2010).
[29] M.-T. Suzuki, N. Magnani, and P. M. Oppeneer, Phys. Rev. B **88**, 195146 (2013).
[30] X. Wang, J. R. Yates, I. Souza, and D. Vanderbilt, Phys. Rev. B **74**, 195118 (2006).
[31] D. Gosálbez-Martínez, I. Souza, and D. Vanderbilt, Phys. Rev. B **92**, 085138 (2015).
[32] Z. Fang, N. Nagaosa, K. S. Takahashi, A. Asamitsu, R. Mathieu, T. Ogasawara, H. Yamada, M. Kawasaki, Y. Tokura, and K. Terakura, Science **302**, 92 (2003).
[33] M. Onoda and N. Nagaosa, J. Phys. Soc. Jpn. **71**, 19 (2002).
[34] T. Jungwirth, Q. Niu, and A. H. MacDonald, Phys. Rev. Lett. **88**, 207208 (2002).
[35] D. J. Thouless, M. Kohmoto, M. P. Nightingale, and M. Den Nijs, Phys. Rev. Lett. **49**, 405 (1982).
[36] M.-C. Chang and Q. Niu, Phys. Rev. B **53**, 7010 (1996).
[37] G. Sundaram and Q. Niu, Phys. Rev. B **59**, 14915 (1999).
[38] Generalization of the definition for commensurate magnetic order with $\boldsymbol{q} \neq 0$ is straightforward by considering the magnetic unit cell expanded from the crystal unit cell.
[39] R. Shiina, H. Shiba, and P. Thalmeier, J. Phys. Soc. Jpn. **66**, 1741 (1997).
[40] A. Kiss and P. Fazekas, Phys. Rev. B **71**, 054415 (2005).
[41] T. Takimoto, J. Phys. Soc. Jpn. **75**, 034714 (2006).
[42] M.-T. Suzuki and H. Ikeda, Phys. Rev. B **90**, 184407 (2014).
[43] S. Tomiyoshi, J. Phys. Soc. Jpn. **51**, 803 (1982).
[44] P. Brown, V. Nunez, F. Tasset, J. Forsyth, and P. Radhakrishna, J. Phys.: Condens. Matter **2**, 9409 (1990).
[45] S. Tomiyoshi and Y. Yamaguchi, J. Phys. Soc. Jpn. **51**, 2478 (1982).
[46] T. Nagamiya, S. Tomiyoshi, and Y. Yamaguchi, Solid State Commun. **42**, 385 (1982).
[47] Experiments observe a tiny net magnetization $M \sim 0.002\mu_B$, most likely due to the deviation of the magnetic structure.
[48] We only consider the contribution of the spin moments for the CMPs in Eq. (6) and (7), since the orbital moments are negligible due to the small S-O in the 3*d*-electron systems.
[49] P. Giannozzi, S. Baroni, N. Bonini, M. Calandra, R. Car, C. Cavazzoni, D. Ceresoli, G. L. Chiarotti, M. Cococcioni, I. Dabo, *et al.*, J. Phys.: Condens. Matter **21**, 395502 (2009).
[50] J. P. Perdew, K. Burke, and M. Ernzerhof, Phys. Rev. Lett. **77**, 3865 (1996).
[51] A. A. Mostofi, J. R. Yates, Y.-S. Lee, I. Souza, D. Vanderbilt, and N. Marzari, Comput. Phys. Commun. **178**, 685 (2008).
[52] Y. Yao, L. Kleinman, A. H. MacDonald, J. Sinova, T. Jungwirth, D.-s. Wang, E. Wang, and Q. Niu, Phys. Rev. Lett. **92**, 037204 (2004).